Rarefaction waves, solitons, and holes in a pure electron plasma

J. D. Moody[a] and C. F. Driscoll
Department of Physics, University of California, San Diego, La Jolla, California 92093

(Received 21 July 1995; accepted 31 August 1995)

The propagation of holes, solitons, and rarefaction waves along the axis of a magnetized pure electron plasma column is described. The time dependence of the radially averaged density perturbation produced by the nonlinear waves is measured at several locations along the plasma column for a wide range of plasma parameters. The rarefaction waves are studied by measuring the free expansion of the plasma into a vacuum. A new hydrodynamic theory is described that quantitatively predicts the free expansion measurements. The rarefaction is initially characterized by a self-similar plasma flow, resulting in a perturbed density and velocity without a characteristic length scale. The electron solitons show a small increase in propagation speed with increasing amplitude and exhibit electron bursts. The holes show a decrease in propagation speed with increasing amplitude. Collisions between holes and solitons show that these objects pass through each other undisturbed, except for a small offset. © *1995 American Institute of Physics.*

I. INTRODUCTION

Large-amplitude (nonlinear) electron plasma wave disturbances of a magnetized plasma column represent a type of plasma behavior that is rich in interesting physics phenomena. Three of these phenomena, which have been studied in detail in neutral plasmas, are (1) electron plasma solitons,[1–3] (2) electron holes,[3–6] and (3) electron plasma shock waves.[7] Here, we experimentally investigate holes, solitons, and rarefaction waves in a pure electron plasma. The large-amplitude electron rarefaction wave has received considerable theoretical attention in neutral plasmas,[8–11] but little experimental study in either neutral or non-neutral plasmas. This rarefaction wave is produced by the free expansion of an electron plasma column along the axial magnetic field. We present a detailed description of the free expansion and add to this a description of a new hydrodynamic theory that quantitatively predicts the measurements. In contrast, the soliton and hole study is mainly phenomenological, in that we only describe the character of these nonlinear objects.

The rarefaction wave consists of a wave front propagating into an undisturbed plasma. Behind the front, the plasma density smoothly decreases while the plasma flow speed increases. A physical picture of the nonlinear effects that lead to a rarefaction wave can be made by considering the hydrodynamic properties of the plasma. The local wave phase speed in the plasma mostly depends on the local electron density and flow speed. Two adjacent parts of the rarefaction wave propagate at slightly different speeds as a result of the smooth decrease in the plasma density associated with the wave; the higher-density part propagates slightly faster than the lower-density part. Because the rarefaction wave propagates from low to high density, the lower-density part of the wave cannot keep up with the higher-density faster moving part, so the wave spreads out. The opposite situation, in which a wave propagates from high to low density, would lead to a shock wave. This description of the nonlinear evolution of the plasma density is analogous to the description of the spreading or steepening of pressure waves in a compressible fluid.[12]

We observe that the rarefaction front propagates into the plasma at the phase velocity of the longest electron–plasma waves, V_{ep}. After the front has passed, the electron density asymptotes to a "plateau" value of 0.55 times the original density. When the front reflects from the far end of the apparatus, the electron density decreases toward zero.

A hydrodynamic model incorporating the full radial profile of the rarefaction front is developed. This model predicts a self-similar rarefaction front, in quantitative agreement with the measurements.

Wave steepening and dispersion are important in describing a soliton in a bounded cylindrical plasma. The soliton is a localized positive density perturbation that retains its shape as it propagates. It travels with a speed greater than the local plasma wave phase speed, and can be described by considering only the hydrodynamic properties of the plasma. Short-wavelength plasma modes are predominantly present in the soliton as a result of its narrow spatial extent. Dispersion of these short-wavelength modes, resulting from the cylindrical plasma geometry, tends to cause a spreading of the narrow density perturbation. This tendency to spread is balanced by the nonlinear effect of wave steepening. What results is a steady-state object that retains its shape.

We observe positive density solitary perturbations to propagate for up to ten axial transits of the apparatus, at a speed slightly above V_{ep}. Large-amplitude solitons seem to be accompanied by an electron burst that propagates up to 1.8 times the electron–plasma wave phase velocity.

A full description of an electron hole must take into account the kinetic properties of the plasma. A hydrodynamic description alone predicts the evolution of the hole into a wavetrain, but this is not what is observed in the experiments described here and elsewhere. The hole persists for 50–100 transits of the apparatus, and consists of a localized negative density perturbation containing a group of electrons trapped in the relatively positive potential of the hole. These trapped electrons can be described as a hollow vortex in phase space.

[a]Present address: Lawrence Livermore National Laboratory, P.O. Box 5508, Livermore, California 94550.

 1070-664X/95/2(12)/4482/12/$6.00

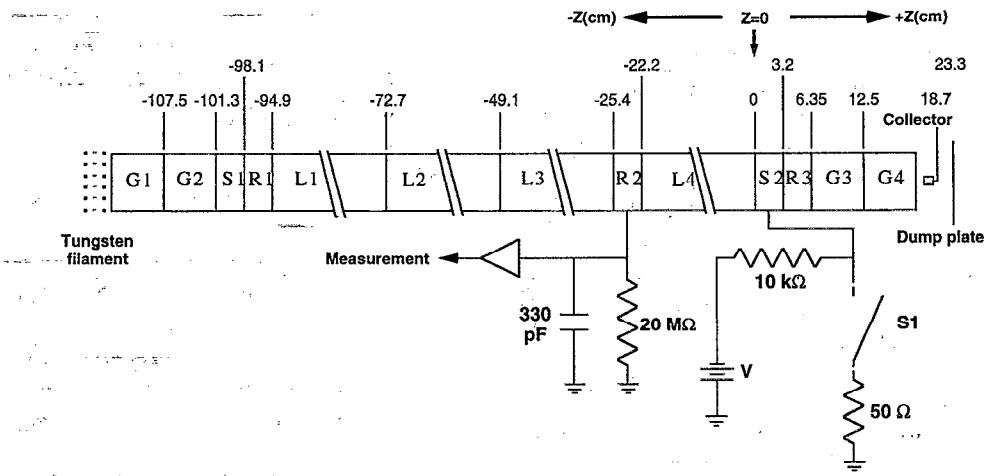

FIG. 1. Cut-away view showing the conducting ring structure of the experimental apparatus, as well as the circuits used to initiate plasma free expansion and measure image charge signals on the confinement rings.

Plasma wave dispersion does not play an important role in the evolution of the electron hole. The holes are observed to propagate at less than V_{ep}. Finally, we observe that solitons and holes are robust, in that they pass through each other, retaining their identity.

The outline of the remainder of this paper is as follows. In Sec. II we describe the experimental apparatus and the processes of initiating the plasma free expansion and exciting solitons and electron holes. The measurements of the free expansion are presented in Sec. III. In Sec. IV we discuss two analytical models for free expansion. In Sec. V we describe the measurements of the electron holes and solitons, and discuss several comparisons between neutral plasma and pure electron plasma holes and solitons. The conclusions are presented in Sec. VI.

II. EXPERIMENTAL APPARATUS AND PROCEDURES

Figure 1 shows a schematic of the experimental apparatus used in this study. The pure electron plasma column is contained radially by a uniform axial magnetic field B and axially by electrostatic potentials V_C applied to segments of a conducting cylinder surrounding the plasma. The properties of a pure electron plasma confined in this type of device have been extensively investigated.[13] The conducting cylinder diameter is $2R_W=6.1$ cm. The plasma radial density profile is typically bell shaped with a full width half-maximum (FWHM) of about 3 cm. Confinement potentials of -50 to -150 V are applied to rings G1 and S2, and the resulting plasma column is about 101 cm long.[14] The experiments were conducted with the following plasma parameters: axial magnetic field 280 $G\leqslant B\leqslant 630$ G; central plasma density 3×10^6 cm$^{-3}\leqslant n_0\leqslant 8\times10^6$ cm^{-3}, space charge potential on axis of $\phi_s\simeq -12$ V for $n_0=7\times10^6$ cm^{-3} (estimated from the measured radial density profile); parallel electron temperature 1 eV$\leqslant\kappa T_\parallel\leqslant$18 eV; electron collision frequency 6 s$^{-1}\leqslant\nu_{ee}\leqslant 7\times10^2$ s^{-1}; plasma rotation frequency 0.7×10^5 s$^{-1}\leqslant\nu_r\leqslant 4\times10^5$ s^{-1}; electron bounce frequency $\nu_b\sim 4\times10^5$ s^{-1} (at 1.6 eV); and background neutral pressure of $\sim 6\times10^{-10}$ Torr. While the axial confining potentials and magnetic field are applied, background transport of the plasma causes n_0 to decrease to one-half of its initial value in about 0.2 s.

The plasma typically undergoes a three-stage cycle consisting of injection, hold, and dump. During injection, a negative axial confining potential is applied to S2, and G1 is grounded, allowing electrons from the hot tungsten filament to fill the confinement region. The hold stage begins when a negative potential is applied to G1, trapping the electrons in the confinement region for the duration of the hold cycle. The dump cycle is initiated when S2 is grounded. The electron column then expands out of the confinement region, and is collected by the dump plate located several centimeters beyond G4. This plate is biased at a constant $+90$ V in order to reduce the effect of secondary electron emission. The typical cycle-to-cycle variation in plasma parameters is about 0.1%. A small circular metal cup with radius $\frac{5}{64}$ in., which is continuously movable in the radial direction, is used to collect a sample of the escaping charge when the plasma is dumped. The approximate plasma density as a function of radius is obtained by dividing this collected charge by the product of the cup area and the estimated plasma column length.

The plasma temperature at the beginning of the hold cycle is typically 1 eV$\pm$0.1 eV. This temperature is determined by measuring the initial rate at which charge escapes when the confinement potential is switched to a series of intermediate values between ground and the initial confinement potential.[15] This measurement provides sufficient data to determine the parallel energy distribution function, from which the temperature can be obtained. Compressional heating of the plasma is sometimes used to increase the temperature up to a maximum of 18 eV. This is done by applying a 10 kHz square wave voltage, which oscillates between ground and -40 V, to either ring L1 or L4. The signal is applied for up to 40 ms to obtain the desired final temperature. Plasma heating above 10 eV generally increases the

plasma density slightly (due to ionization of the background neutrals), and produces only minor radial profile changes.

Changes in the radially averaged plasma density at a particular axial location are detected by monitoring the induced image charge on a confinement ring at the corresponding axial position, as shown by the circuit connected to R2 in Fig. 1. The ring is connected to the input of a low noise, 30 db inverting amplifier with a 5 MHz bandwidth. The total amplifier input capacitance is about 3.3×10^{-10} F, and the input is connected to ground through a 20 MΩ resistor. Electron plasma injection causes a voltage of -10 to -20 mV to appear on the amplifier input. This voltage exponentially decays to 0 with a RC time constant of about 6 ms. An image charge, Q_0, remains on the ring during the hold cycle, with Q_0 equal and opposite to the total charge contained in a length of plasma equal to the length of the ring.

The free expansion is initiated by grounding the confinement ring S2 using the circuit shown in Fig. 1. A mechanical relay gives a switching time of approximately 25 ns; bouncing of this switch is unimportant because the plasma is completely dumped before this can occur. As the plasma expands out of the confinement region, positive image charge begins to leave the detector ring (R2) giving a positive voltage at the amplifier input. This voltage is proportional to $Q(t)-Q_0$ for times short compared to the 6 ms RC decay time. The quantity $Q(t)$ represents the total charge at time t contained in a length of plasma equal to the ring length. The amplified and inverted output is then digitized, normalized to $|Q_0|$ and offset by unity, giving a signal equal to $Q(t)/Q_0$.

The charge $Q_{r=0}(t)$ that escapes at $r=0$ is measured with a centered collector located between G4 and the dump plate. The collected charge is measured with the same type of inverting amplifier as used for the R2 signals, and is normalized to the total charge collected on center $Q_{r=0}$.

Excitation of electron holes and solitons is accomplished by applying voltage steps or pulses to R3. The pulses have variable amplitude ($-100\ \text{V}\leq V_0\leq 100\ \text{V}$) and variable width ($20\ \text{ns}\leq\tau\leq 10$ ms), with rise times of about 20 ns. If the voltage step is negative, a soliton develops, provided that the magnitude of the step is large enough. An electron hole results if the voltage step is large and positive. These holes and solitons are studied in a plasma confined between rings G2 and G3.

III. FREE EXPANSION MEASUREMENTS

Figure 2 shows the image charge signals measured on rings R1, R2, and G3, and the confinement voltage applied to ring S2 as a function of time for a typical plasma free expansion. When the confinement voltage on S2 is grounded, the signal on R2 remains unchanged for a short time, then drops quickly and approaches a plateau level with a value nearly equal to $\frac{1}{2}$. The short delay before the R2 signal begins to drop corresponds to the time for the rarefaction front to propagate from the position of ring S2 to ring R2. There is a longer delay of about 720 ns before the signal on ring R1 begins to drop. The propagation speed of the front is calculated to be $c=96.5$ cm/720 ns$=1.3\times10^8$ cm/s. The G3 signal is initially zero, but begins to rise approximately 50 ns after S2 is grounded, approaching the same plateau value approached by R2. The signal on G3 is measured the same way as the other ring signals; however, the normalized (digitized) amplifier output is not offset by unity.

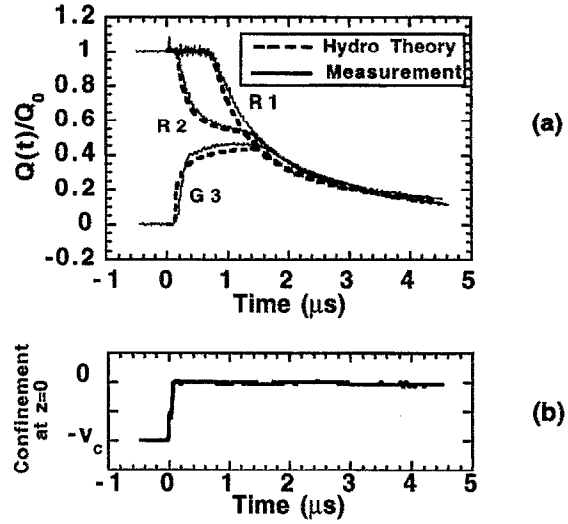

FIG. 2. (a) Measured signals on R1, R2, and G3 as a function of time for a typical plasma free expansion compared with the predictions of the hydrodynamic model. (b) The measured confinement voltage applied to ring S2.

Separate measurements of the front propagation speed between R3 and R2 and between R2 and R1 for various choices of confinement rings indicate that the front propagates at a uniform speed throughout the plasma column. By the time the front has reached the far end of the column at G2, the density decrease in the rarefaction disturbance extends smoothly from G2 to G4. This is in contrast to the much more localized density variation of an electron hole or soliton with a measured scale length of five to six times the plasma diameter. The signals on R2 and G3 remain close to the plateau value until the rarefaction front returns from reflection off of the confined end of the plasma column. At this time, both the R2 and G3 signals drop below the plateau value, with R2 dropping slightly earlier than G3. The three signals from R1, R2, and G3 then merge as they asymptotically approach zero. The R1 signal at the confined end of the column does not exhibit a plateau value but drops smoothly to zero.

Figure 3 shows the normalized escaped charge $Q_{r=0}(t)$ on the cylinder axis as a function of time. Following a short initial delay, there is a linear charge increase that continues until the rarefaction front has reflected from the confined plasma end and traveled back to the front of the plasma column. The escaping charge then no longer increases linearly but asymptotically approaches the total charge initially contained along the axis of the plasma column.

The rarefaction front propagates through the undisturbed plasma at the electron plasma wave phase speed V_{cp}. Figure 4 shows the measured speed of the rarefaction front as a function of central plasma density n_0 for a low and high plasma temperature. Also shown in the figure is the calculated speed of small-amplitude long-wavelength electron plasma waves in the same column determined using the mea-

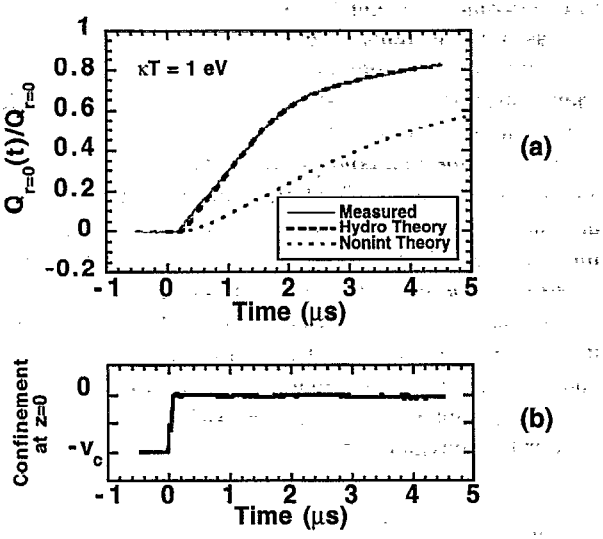

FIG. 3. (a) Measured collected charge at $r=0$ for plasma free expansion compared with the predictions of the hydrodynamic model and the noninteracting neutral gas model for a temperature of 1 eV. (b) The measured confinement voltage applied to ring S2.

sured electron density radial profile.[16,17] The discrepancy between the measured and calculated speeds at high temperature and density is most likely due to the 10% typical uncertainty in the measured electron temperature; the data lies between the curves calculated for 13.5 and 16.5 eV. One result of the increase in speed of the rarefaction front with higher electron temperature and density is that the characteristic signal features on rings R2 and R1 (such as the initial signal drop and the fall away from the plateau value) occur earlier in time for higher density or temperature plasma.

The plateau density n_p is measured to be about one-half of the initial density for a wide range of plasma parameters. Figure 5 shows the ratio n_p/n_0 as a function of plasma density for four different magnetic fields. The quantity n_p is the value of the R2 signal in the plateau region, and n_0 is the maximum value of the R2 signal. The ratio n_p/n_0 is 0.55 ± 0.02 over the entire range of experimental densities and magnetic fields. The hydrodynamic model described in Sec.

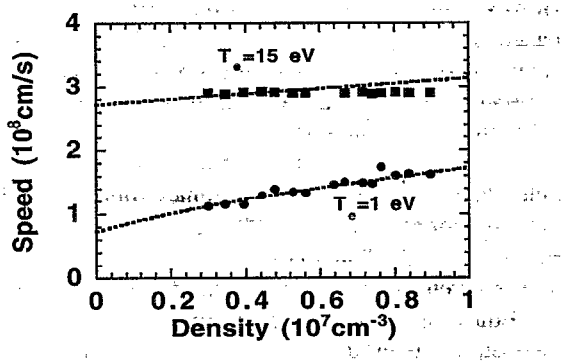

FIG. 4. Propagation speed of the rarefaction front as a function of central plasma density for 1 and 15 eV. The dotted lines show the calculated speed of small-amplitude long-wavelength plasma waves.

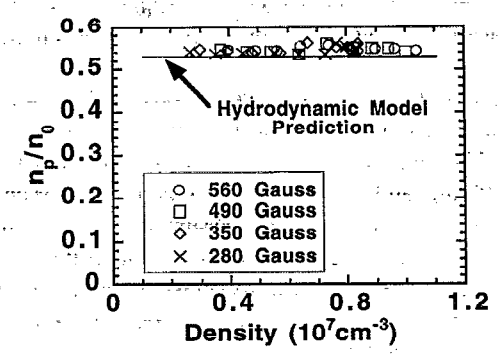

FIG. 5. Ratio n_p/n_0 as a function of central plasma density for a number of magnetic fields. The maximum signal on R2 is n_0 and the plateau value is n_p.

IV predicts a value of n_p/n_0 that is 0.53 and is independent of the plasma density, magnetic field, and temperature.

Summarizing the measurements of the plasma free expansion, we find that when the confining potential is grounded, a rarefaction disturbance begins to propagate into the plasma column. The front of this disturbance propagates at the phase speed of long-wavelength electron plasma waves. The plasma density behind the front decreases over a long distance to a plateau value with a radially averaged density that is ~one-half of the initial radially averaged density. The front reflects from the confined end of the plasma column, causing the density to continue decreasing, eventually emptying the confinement region of plasma. As the plasma density or temperature is increased, the observations change in a way that is consistent with the increasing propagation speed of the disturbance. The plasma mostly empties from the confinement region in the time it takes a long-wavelength electron plasma wave to traverse the length of the plasma column several times.

IV. ANALYTICAL MODELS OF PLASMA FREE EXPANSION

In the free expansion, the electrons escape from the confinement region as a result of (1) electrostatic "pressure" and (2) ballistic free streaming. The comparative importance of these two effects depends on the ratio λ_D/a, where λ_D is the plasma Debye length and a is the plasma radius. Electrostatic effects dominate for $\lambda_D/a \ll 1$, and kinetic effects dominate when $\lambda_D/a \gg 1$.

In this section we describe two models for the plasma free expansion. The first is a noninteracting neutral gas model that would be applicable in the limit of no electrostatic effects (i.e., a high-temperature plasma). This model predicts results that do not agree well with the measurements at either the low- or high-temperature range, but show a tendency toward better agreement at a higher temperature ($\kappa T \gtrsim 15$ eV at $n_0 \sim 1\times 10^7$ cm^{-3} and $a \sim 1.5$ cm). This model is simple to derive and is useful for predicting the importance of ballistic free streaming. Electrostatic pressure must be included in the dynamics for the entire experimental range of electron temperatures (1 eV $< \kappa T < 15$ eV), since $\lambda_D/a < 0.7$. A new hydrodynamic theory of nonlinear plasma

wave evolution in a bounded cylinder quantitatively predicts the measurements at these low to moderate plasma temperatures.

The initial and boundary conditions for both models are the same. The plasma column is confined between $z=0$ and $z=-L$. The plasma density is assumed to be uniform along each field line, and to fall abruptly to zero at either end of the plasma column. The plasma is assumed to have zero initial fluid velocity. At time $t=0$ the confinement voltage at $z=0$ is instantaneously removed and the plasma begins to freely expand. An initially constant radial temperature profile is assumed in both models.

A. Noninteracting neutral gas model

This model, which only approximates the measurements for a hot plasma ($\lambda_D/a \gg 1$) treats the electrons as a neutral noninteracting gas. The electrostatic collective effects are completely neglected, and the plasma expansion is assumed to result only from electron thermal motion. We assume that the plasma initially has a Maxwellian distribution of velocities with a temperature T, and that the electrons are specularly reflected from the confined plasma end ($z=-L$). These assumptions lead to a plasma density and average velocity in the confinement region ($-L \leqslant z \leqslant 0$), given by

$$n(r,z,t)=\tfrac{1}{2}n_0(r)[\mathrm{erf}(\alpha_1)+\ \mathrm{erf}\ (\alpha_2)], \tag{1}$$

$$v(r,z,t)=\frac{1}{2\sqrt{\pi}}\frac{n_0(r)}{n(r,z,t)}(\ \exp[-\alpha_1^2]-\ \exp[-\alpha_2^2]), \tag{2}$$

$$\alpha_1(z,t)\equiv\frac{|z|}{tv_t}, \tag{3}$$

$$\alpha_2(z,t)\equiv\frac{2L+z}{tv_t}. \tag{4}$$

Here, $n_0(r)$ is the initial density profile, $v_t=\sqrt{2\kappa T/m}$ is the electron thermal speed, and $\mathrm{erf}(x)$ is the standard error function.[18] These results are similar to those given in Ref. 19.

Comparison between the measured image charge $Q(t)/Q(0)$ and that predicted by the noninteracting neutral gas model for a plasma with an initially constant radial temperature of 1 eV$\pm$0.15 eV shows poor agreement. [The linear charge density contained within a confinement cylinder is $\sigma(z,t)\equiv\int 2\pi r dr n(r,z,t)$, and the image charge measured on a cylinder at z is proportional to this quantity.] Agreement between measurement and theory is improved at high plasma temperatures ($T=15\pm2$ eV), although there is still substantial discrepency. The disagreement in both cases results because the plasma escapes from the confinement region faster than the noninteracting neutral gas model predicts. This is an indication that the electrostatic effects play a role that is at least comparable to the kinetic effects in removing electrons from the confinement region, even for a plasma temperature of 15 eV.

B. Hydrodynamic model

We have developed a new theory based on the hydrodynamic characteristics of the plasma that contains the physics of electrostatic and kinetic pressure. As the plasma expands, it is assumed to remain describable by equilibrium thermodynamics and continuum conservation laws. Previously, Manheimer presented a simple hydrodynamic model for the nonlinear steepening of an electron plasma wave in a bounded cylindrical cold plasma.[20] He expanded the nonlinear solution in terms of solutions of the linearized equations and neglected coupling between separate radial and azimuthal modes. Here, we describe a hydrodynamic model that determines the exact radial evolution during free expansion of a bounded cylindrical warm plasma. Finite temperature is included by a scalar pressure term in the momentum conservation equation and an adiabatic equation of state.

The plasma dynamics are described by the following set of four hydrodynamic equations:

$$\frac{\partial n}{\partial t}=-\frac{\partial}{\partial z}(nv), \tag{5}$$

$$\frac{\partial v}{\partial t}=-v\frac{\partial v}{\partial z}+\frac{e}{m}\frac{\partial\phi}{\partial z}-\frac{1}{mn}\frac{\partial P}{\partial z}, \tag{6}$$

$$\nabla_\perp^2\phi\simeq\nabla^2\phi=4\pi en, \tag{7}$$

$$\frac{d}{dt}\left(\frac{P}{n^\gamma}\right)=0. \tag{8}$$

Here, ϕ is the plasma potential, v is the local axial fluid velocity, and P is the local pressure; m is the electron mass, and $-e$ is the electron charge. The magnetic field confines particle motion to be axial, so the ratio of specific heats is $\gamma=3$. We assume cylindrical symmetry in the theory, since wall sector measurements indicate no detectable azimuthal asymmetries.

The density, potential, and pressure are written as

$$n(r,z,t)\equiv\xi(r)[n_0+\delta n(r,z,t)]\equiv\xi(r)\bar{n}(r,z,t), \tag{9}$$

$$\phi(r,z,t)=\phi_0(r)+\delta\phi(r,z,t), \tag{10}$$

$$P(r,z,t)=\xi(r)[P_0+\delta P(r,z,t)]. \tag{11}$$

Here, $\xi(r)$ gives the equilibrium radial density dependence with $\delta n(r,z,0)=0$; n_0, P_0, and ϕ_0 are the equilibrium density, pressure, and space charge potential on axis; and δn, $\delta\phi$, and δP are the perturbed density, potential, and pressure. The perturbed quantities are not constrained to be small. However, the axial variation of the rarefaction density disturbance in a length of one plasma radius is assumed to be small. This allows $\nabla^2\phi$ in the Poisson equation (7) to be replaced with $\nabla_\perp^2\phi$. This approximation greatly simplifies the solution of the system (5)–(8).

Equation (8) indicates that the plasma entropy per particle (P/n^3) remains constant (homentropic flow) along each field line for all times. This allows us to write the last term in Eq. (6) as $-(3\kappa T/m)(1/\bar{n})\partial\bar{n}/\partial z$, where the local temperature is given in terms of the local density as $T=T_0(\bar{n}/n_0)^2$.

Equations (9)–(11) are substituted into Eqs. (5)–(8) and then Eq. (8) is used in Eq. (6) to give the three equations:

$$\frac{\partial\bar{n}}{\partial t}=-\bar{n}\frac{\partial v}{\partial z}-v\frac{\partial\bar{n}}{\partial z}, \tag{12}$$

$$\frac{\partial v}{\partial t}=-v\frac{\partial v}{\partial z}+\frac{e}{m}\frac{\partial \phi}{\partial z}-\frac{3\kappa T}{m}\frac{1}{\bar{n}}\frac{\partial \bar{n}}{\partial z}, \tag{13}$$

$$\frac{1}{r}\frac{d}{dr}r\frac{d\phi}{dr}=4\pi e n, \tag{14}$$

where κ is the Boltzmann constant. Equations (12) and (13) describe the plasma dynamics along individual magnetic field lines (at constant r) and Eq. (14) radially couples the dynamics along each field line.

The initial and boundary conditions assumed in this model lead to a solution that possesses no scale length for times earlier than the time it takes the rarefaction front to reach $z=-L$. As a result, the solution to Eqs. (12)–(14) is self-similar in nature,[21] with z and t appearing only as the ratio z/t. The self-similar solution to Eqs. (12)–(14) is obtained as follows. The ratio z/t is written as $\zeta \equiv z/t$ and the partial derivatives with respect to space and time are written as

$$\frac{\partial}{\partial z}=\frac{1}{t}\frac{d}{d\zeta} \quad \text{and} \quad \frac{\partial}{\partial t}=-\frac{1}{t}\zeta\frac{d}{d\zeta}. \tag{15}$$

The continuity equation now becomes

$$\frac{d\bar{n}}{dv}=\frac{\bar{n}}{\zeta-v}, \tag{16}$$

and the momentum equation (13) is written using Eq. (16) as

$$(\zeta-v)^2-\left[\frac{3\kappa T_0}{m}\left(\frac{\bar{n}}{n_0}\right)^2-\frac{e}{m}\bar{n}\frac{d\phi/d\zeta}{d\bar{n}/d\zeta}\right]=0. \tag{17}$$

Equation (17) relates the local gradient of the potential ($d\phi/d\zeta$) to the local gradient of the density ($d\bar{n}/d\zeta$) along a field line. The radial dependence of $d\phi/d\zeta$ and $d\bar{n}/d\zeta$ are determined by the Poisson equation. Equation (17) is solved for $d\bar{n}/d\zeta$, which is then used in the ζ derivative of the Poisson equation to give

$$\frac{1}{r}\frac{d}{dr}r\frac{d}{dr}\left[\frac{d\delta\phi}{d\zeta}\right]+\frac{\bar{\omega}_p\xi(r)}{(\zeta-v)^2-(3\kappa T_0/m)(\bar{n}/n_0)^2}\left[\frac{d\delta\phi}{d\zeta}\right]=0, \tag{18}$$

where $\bar{\omega}_p=4\pi\bar{n}e^2/m$. Equation (18) is an eigenvalue equation for $d\phi/d\zeta$, where ζ is the eigenvalue and $d\phi/d\zeta$ is the eigenfunction. Here $d\phi/d\zeta$ is zero at the conducting wall, $r=R_w$, and regular at $r=0$.

The solution to Eq. (18) gives a single function for the plasma potential ($d\phi/d\zeta$) in terms of r and ζ; all the other macroscopic plasma parameters can be derived from ϕ and Eqs. (16) and (17). Equation (18) has the same form as the eigenvalue equation obtained by solving the fluid equations for the potential of an azimuthally symmetric, linear electrostatic plasma wave in a cylindrical plasma with equilibrium density $\bar{n}\zeta(r)$ and flow velocity v. The self-similar nature of the solution indicates that each part of the rarefaction disturbance propagates into (or out of) the plasma with a velocity given by ζ (this is the local phase velocity of the rarefaction wave).

There is an infinite family of eigenfunction solutions to Eq. (18), each characterized by the number of radial nodes in the eigenfunction. There are two eigenvalue–eigenfunction pairs for a given number of nodes in the radial eigenfunction. The two eigenvalues correspond to plasma waves propagating either along the $-\hat{\mathbf{z}}$ or $+\hat{\mathbf{z}}$ direction. If the plasma flow velocity is very large, both waves may propagate in the same direction; however, one will have a larger phase velocity than the other. Since the rarefaction wave is measured to initially propagate in the $-\hat{\mathbf{z}}$ direction (in the geometry described here) the correct choice for the eigenvalue ζ is given by the lesser of the two eigenvalues obtained by solving Eq. (18).

The rarefaction front is identified as the boundary separating the unperturbed plasma from the perturbed plasma. Experimentally, this front is measured to propagate at the fastest azimuthally symmetric electron plasma wave phase speed.[22] In order to match this observation, the solution to Eq. (18) with no radial nodes is used to construct the self-similar solution. It is helpful to note that the dispersion relation for the long-wavelength electron plasma modes is acoustic-like so that the frequency ω is proportional to the wave number k. This means that the phase speed and the group speed are equal for these modes. It is interesting that at $\zeta=0$, the self-similar nature of the solution indicates that the local wave phase velocity (equal to ζ) is also zero. For $\zeta=0_+$ the phase velocity is positive and for $\zeta=0_-$ the phase velocity is negative. This means that during self-similar plasma flow, a small-amplitude plasma disturbance excited on top of the rarefaction wave in the region $\zeta>0$ cannot propagate past $\zeta=0$ into the region where $\zeta<0$. We have tested this experimentally and will discuss it in Sec. IV C. This condition remains true only during self-similar plasma flow, which lasts until the reflected front returns to the position $\zeta=0$.

The self-similar solution described by Eqs. (17) and (18) cannot be determined analytically, so we evaluate it numerically. This is done by integrating the continuity equation (16) and the momentum equation (17) together with the Poisson equation (18), to determine the solution as a function of r at successive values of ζ. The continuity equation can be integrated analytically to give $\bar{n}/n_0=c_0/(v-\zeta)$, where c_0 is the rarefaction front speed. Using this relation between $\bar{n}$ and v, Eqs. (17) and (18) are rewritten as

$$\frac{d\bar{n}}{d\zeta}=\frac{\bar{n}}{\bar{v}_t(\bar{n}/n_0)^2-(c_0n_0/\bar{n})^2}\frac{e}{m}\frac{d\phi}{d\zeta}, \tag{19}$$

$$\frac{1}{r}\frac{d}{dr}r\frac{d}{dr}\left[\frac{d\phi}{d\zeta}\right]+\frac{\bar{\omega}_p\xi(r)}{(c_0n_0/\bar{n})^2-\bar{v}_t(\bar{n}/n_0)^2}\left[\frac{d\phi}{d\zeta}\right]=0. \tag{20}$$

The solution to Eq. (20) at a particular ζ gives the radial dependence of $d\phi/d\zeta$, but does not determine its overall amplitude. The initial condition that the rarefaction front is located at $\zeta=-c_0$ fixes this amplitude to be

$$\left.\frac{d\phi}{d\zeta}\right|_{\zeta=-c_0}=\frac{\phi_0}{c_0}f(r). \tag{21}$$

Here, $f(r)$ is the radial eigenfunction from the solution of Eq. (20), normalized so that $f(r=0)=1$. This initial condition for $d\phi/d\zeta$ can now be used in the integration of Eqs. (19) and (20) to give $\bar{n}$ and ϕ as a function of ζ and r.

The general numerical procedure for integrating Eqs. (19) and (20) is as follows. The solution region is divided into 51 radial points from $-a \leq r \leq a$ and 81 points from $-c_0 \leq \zeta \leq 1.6c_0$. The value of $1.6c_0$ is chosen as the maximum value of ζ in the solution region since the behavior of the plasma in the region beyond this point ($\zeta > 1.6c_0$) has no effect on the solution where $\zeta \leq 0$ and at times for which a comparison is made with the experimental results. Equation (20) is solved to obtain $d\phi/d\zeta$ for a given $\bar{n}$. Equation (19) is integrated along a small step in ζ using the current value for $d\phi/d\zeta$ to obtain a new value for $\bar{n}$. This new value of $\bar{n}$ is used in Eq. (20) to determine the new value of $d\phi/d\zeta$ and the step-by-step numerical solution process continues. The actual solution procedure uses a 12th-order predictor–corrector integration scheme. The solution gives $\bar{n}$, v, and ϕ as functions of ζ. The actual solution for $\bar{n}$, v, and ϕ as a function of z and t can then be determined from these three functions and the relation $\zeta = z/t$.

At times before the rarefaction front reaches $z = -L$, the large-amplitude plasma perturbation consists of simple waves; that is, only the waves satisfying Eq. (18) with the lesser phase velocity are present in the plasma. The boundary condition at $z = -L$ is that the plasma flow velocity is kept at zero. This causes a reflection to occur when the rarefaction front reaches this point. The reflected front propagates back through the perturbed plasma at a velocity

$$\frac{dz}{dt} = c_+ . \tag{22}$$

Here, c_+ is the local plasma wave phase velocity, which is now the greater of the two possible phase velocities of waves satisfying Eq. (18). The value of c_+ is determined from the density and velocity given by the self-similar solution that is still valid at the reflected front.

The plasma perturbation now evolving between $z = -L$ and the reflected front consists of compound waves; that is, both waves that satisfy Eq. (18) are present. The evolution of the density and velocity in this region is no longer self-similar, so the solution cannot be obtained from Eqs. (19) and (20). However, the solution can be determined using the method of characteristics.[12,23] This method is frequently used to solve large-amplitude hydrodynamic wave problems. The partial differential equations [Eqs. (12)–(14)] are converted to ordinary differential equations along characteristics. Thus,

$$\frac{d\bar{n}}{dt} + \frac{\bar{n}}{c_+ - v}\frac{dv}{dt} = 0, \quad \text{along} \quad \frac{dz}{dt} = c_+ , \tag{23}$$

$$\frac{d\bar{n}}{dt} + \frac{\bar{n}}{c_- - v}\frac{dv}{dt} = 0, \quad \text{along} \quad \frac{dz}{dt} = c_- . \tag{24}$$

Here, $\bar{n}$ is the local density ($n_0 + \delta n$), v is the macroscopic flow velocity, and $c_\pm$ is the plasma wave phase velocity with respect to fixed coordinates. It is straightforward to numerically integrate Eqs. (23) and (24), starting from the self-similar solution obtained from Eqs. (19) and (20) at $t \simeq L/c_0$, to obtain the evolution of $\bar{n}$ and v in the plasma column for long times.

The entire plasma free expansion problem can, in principle, be solved using only the method of characteristics, since the self-similar part of the solution discussed above is a special case of the method of characteristics. However, a numerical solution is required for both the self-similar and method of characteristics solutions, and this is where the self-similar method has an advantage over the method of characteristics. At time $t = 0$ the plasma density has an infinite gradient at $z = 0$. The method of characteristics has an intrinsic scale length associated with the spacing between grid points in the axial direction, and therefore can never accurately resolve the instantaneous drop in the density at $z = 0$. This resolution limit leads to a discrepancy between the plasma evolution predicted by the method of characteristics and the self-similar method. The difference is on the order of 10% in the density prediction, depending on the initial density gradient at $z = 0$ resulting from the choice of grid spacing in the numerical solution. The advantage of the self-similar solution is that it exactly predicts the evolution of the plasma parameters from the initial abrupt drop in the plasma density. In addition, the theory provides useful physical insight into the self-similar nature of the plasma free expansion for early times.

In the limit of a high-temperature plasma, such that electrostatic effects are negligible in comparison to thermal effects, Eqs. (12) and (13) can be solved exactly for the rarefaction disturbance at all times and places. In this case, the fluid equations describe a perfect gas with $\gamma = 3$. As a result, Eq. (17) becomes $(\zeta - v)^2 = 3\kappa T_0/m(\bar{n}/n_0)^2$, and Eq. (16) is integrated analytically to give $v = c_0(1 - \bar{n}/n_0)$ where $c_0 = 3\kappa T_0/m$. The exact self-similar solution for $-1 \leq z/(tc_0) \leq 1$ is given as

$$\frac{\bar{n}}{n_0} = \frac{1}{2}\left(1 - \frac{z}{tc_0}\right), \tag{25}$$

$$\frac{v}{c_0} = \frac{1}{2}\left(1 + \frac{z}{tc_0}\right). \tag{26}$$

The solution for $z/(tc_0) < -1$ is $\bar{n} = n_0$ and $v = 0$; for $z/(tc_0) > 1$ the solution is $\bar{n} = 0$ and $v = 0$. Once the rarefaction front reaches $z = -L$ and reflects, the reflected front propagates back through the already disturbed plasma at exactly the speed $3\kappa T_0/m$. This constant return speed only occurs for the case when $\gamma = 3$. Any other value of γ leads to a nonsteady speed for the reflected front. The solution for the gas density and flow velocity in the region between $z = -L$ and the reflected front is

$$\frac{\bar{n}}{n_0} = \frac{L}{c_0 t} \tag{27}$$

$$\frac{v}{c_0} = \frac{z + L}{c_0 t}. \tag{28}$$

C. Comparisons between the model and the data

The radially averaged density predicted by the new hydrodynamic model is compared with the measurements in Fig. 2. Agreement between the hydrodynamic theory and the data for this low temperature is good. The fluid model closely predicts (1) the time at which the signals on R1, R2, and G3 begin to change; (2) the approach of the signals on R2 and G3 toward a plateau; (3) the duration of this plateau

before the reflected front returns to the location of R2 and G3; and (4) the long time behavior of the signals on R1, R2, and G3. We also find good agreement between the predicted and measured charge escape rate at $r=0$, as is shown in Fig. 3. Agreement between the fluid model and the measurement at moderate plasma temperature ($T_e=15$ eV) is good. This case is not shown here but is shown in Ref. 24. The hydrodynamic model describes the free expansion well in the warm as well as the cold plasma regimes.

We compared our hydrodynamic theory to the Manheimer model, which we modified to include finite temperature. Substantial discrepancy between the two models arises early in the free expansion, when the average density has dropped to just 80% of the average initial density. This indicates that only during very early times is the free expansion adequately described by a model that keeps only the lowest-order linear radial eigenmode. That is, higher-order radial modes, included in the new hydrodynamic model, become important early in the free expansion.

The plateau value at the location of ring R2 just prior to the arrival of the reflected front is calculated numerically from the fluid model to be 0.53 over the entire range of experimental densities, as shown in Fig. 5. This value is in good agreement with the measured value of n_p/n_0, which is about 0.55 for all experimental densities.

We made a number of measurements to determine the sensitivity of our results to the assumptions in the theory. For example, we have varied the end shape of the plasma column by varying the confinement potential from -30 to -180 V, and found only a few percent variation in the measured signals. In addition, we have varied the voltage switching time on the confining ring from about 10 to 100 ns, and found that the measured signals experienced only a shift in time. We also examined the results when the mechanical relay switched the confining ring voltage to a voltage near ground (rather than at ground) ranging from -5 V to $+5$ V (the collector plate remains biased at $+90$ V). No change in the resulting curves is observed for positive voltages, but the curves begin to change slightly for negative voltages less than about -2 V. Finally, using plasma wave heating we have produced a slightly non-Maxwellian initial distribution function and found that this caused only a few percent change in the measured signals.

In addition to these measurements, we have experimentally checked a result of the self-similar solution that was mentioned earlier. This is that small-amplitude waves excited during plasma free expansion in the region $z>0$ cannot propagate into the region $z<0$ for times during which the self-similar solution is valid at $z\sim 0$. Using an experimental arrangement with S2 and G1 as confinement electrodes, S2 is grounded to start the free expansion. As plasma flows out of the confinement region and through rings R3 and G3 to the charge collecting plate, we have applied varying amplitude positive voltage pulses to rings R3 and G3 (where $z>0$) in order to excite low-amplitude plasma waves in the rapidly flowing plasma. During plasma free expansion we have observed no measurable response on inner rings L4, R2, and L3 (where $z<0$).

Summarizing the analytical models for plasma free expansion, we find that the noninteracting neutral gas model predictions never quite agree with the experimental measurements, even in a warm plasma where ($\lambda_D/a=1$), although the agreement improves with increasing temperature. This model retains only kinetic effects, which are expected to dominate electrostatic effects in the high-temperature cases only. The hydrodynamic model agrees well with the measurements over the entire experimental range of density and temperature. Comparison with the predictions of a modified Manheimer model indicates that the plasma evolution is dominated by the lowest-order radial eigenfunction only for very early times and that the higher-order radial eigenfunctions quickly become important in the evolution. The hydrodynamic model predicts a plateau density value at R2 that agrees well with the experimentally measured plateau density.

V. ELECTRON HOLE AND SOLITON MEASUREMENTS

Both positive density perturbation solitons and negative holes can propagate in these plasmas. Most of the characteristics of electron solitons and holes observed in neutral plasmas[1–6] are also seen in the pure electron plasma. For example, the soliton velocity tends to increase with increasing soliton amplitude. The solitons tend to damp more quickly than the electron holes, and two solitons pass through each other while preserving their identity. In addition, the electron hole is remarkably stable, persisting for 50–100 bounce periods in the plasma column. A moderate amplitude hole tends to slough off a smaller hole as it propagates. Also, two electron holes pass through each other while preserving their identity, and a hole seems to exhibit the presence of trapped electrons.

The excitation of holes or solitons in the electron plasma is carried out by applying a voltage step or pulse to a ring adjacent to one of the confinement rings. In the simplest case, the voltage on the ring is switched to a higher (or lower) voltage in about 25 ns and kept there. This rapid change produces either a positive density perturbation (a soliton) if the voltage is switched more negative or a negative density perturbation (a hole) if the voltage is switched less negative. The soliton or hole that is created then propagates back and forth in the plasma column and can be studied as it evolves in time by measuring the image charge signals on the rings along the plasma column.

The propagation of solitons is shown in Fig. 6. Here, a step voltage is applied to ring R3 and the resulting plasma response is measured on ring R1 as a function of time for a plasma contained between rings G2 and G3. The negative voltage step on R3 produces a positive density perturbation, which propagates repeatedly from end to end in the plasma. The signal on R1, which is detected the same way as the rarefaction signals, consists of successive peaks separated by the time it takes the density pulse to propagate from ring G2 to G3 and back to G2.

Increasing the amplitude of the density pulse produces a small but significant increase in the propagation speed, as shown by the solid circles in Fig. 7. This effect can be seen in Fig. 6, where peaks on the upper trace occur slightly earlier in time compared to peaks in the lower trace. The upper trace corresponds to a density perturbation of about 10% and

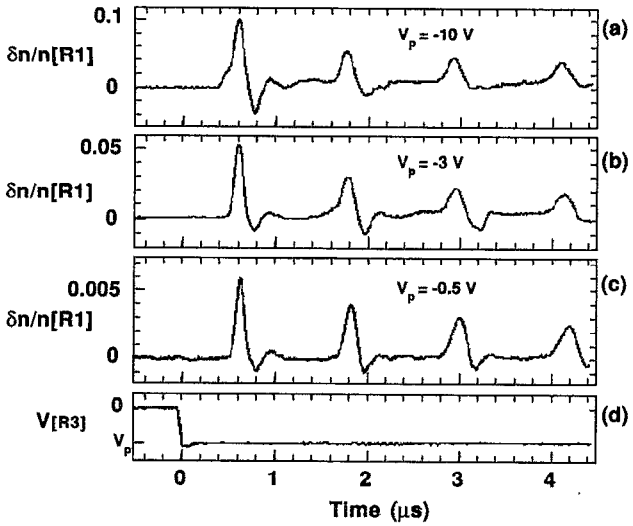

FIG. 6. Resulting plasma density perturbation measured on R1 for (a) large-amplitude, (b) medium-amplitude, and (c) low-amplitude negative step voltages applied to R3. (d) Measured voltage pulse applied to ring R3.

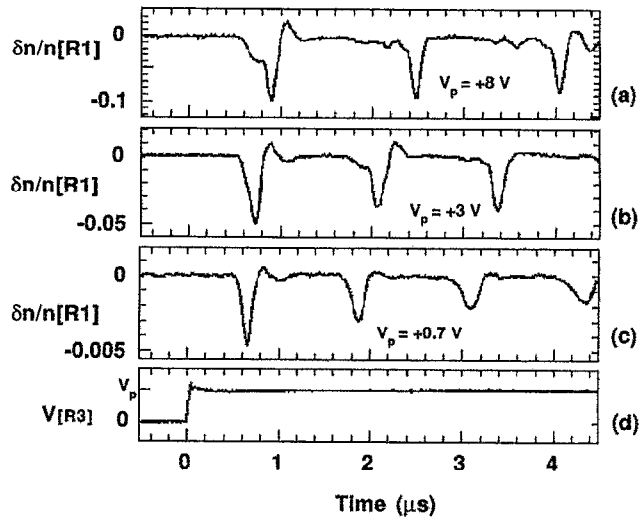

FIG. 8. Resulting plasma density perturbation measured on R1 for (a) large-amplitude, (b) medium-amplitude, and (c) low-amplitude positive step voltages applied to R3. (d) Measured voltage pulse applied to ring R3.

the lower trace is about 0.5%. The largest amplitude solitons we produced experimentally have about a 7% increase in speed over the fastest electron plasma wave. Note that a linear combination of plasma waves still would not propagate faster than the fastest electron plasma wave, so this perturbation is truly nonlinear. Application of a large negative excitation voltage step to R3 does cause a slight shortening of the plasma column length because it increases the confinement potential near G3. This fractional shortening is measured with low-amplitude plasma waves to be a maximum of 2%, so the increase in propagation speed with increasing amplitude is not solely due to the density increase. Further increasing the excitation voltage distorts the end shape of the plasma and complicates the interpretation of the measurements.

At high excitation voltages free-streaming electron bursts[1] are observed. In Fig. 6(a), a $\lesssim -10$ V step pulse on R3 gives a leading edge on the density perturbation signal measured on R1. The velocity of this leading edge is shown as a function of soliton perturbation density in Fig. 7. The speed at large excitation voltages (the density perturbation is not proportional to applied voltage in this regime) is approximately proportional to the square root of the amplitude of the applied step voltage on R3 within experimental uncertainty. Measurement of the parallel electron distribution function of the plasma column after applying a large negative excitation voltage shows a small increase in the number of electrons above the thermal energy. This further confirms the presence of the free-streaming electron burst. The spatial width of the density perturbation is typically about 16–20 cm ($\sim 50\ \lambda_D$) and seems to increase slightly with increasing amplitude.

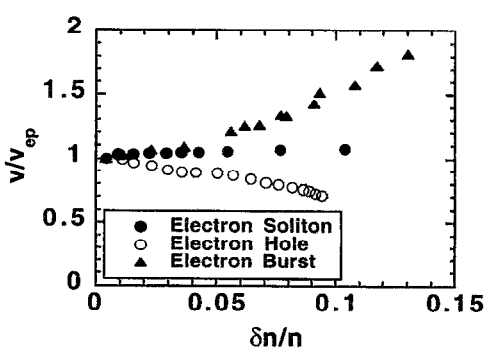

FIG. 7. Propagation speed (normalized to the fastest electron plasma wave speed) of an electron burst, soliton and electron hole as a function of density perturbation amplitude.

Applying a positive voltage step to G3 produces a negative density perturbation referred to by previous authors as an electron hole.[3–6] A very small voltage step produces a linear superposition of electron plasma waves that disperses and damps away over time. Increasing the voltage step above several volts produces a perturbation that disperses and damps much more slowly, and propagates at a speed that is less than the fastest electron plasma wave.

Figure 8 shows successive negative pulses separated by the time required for the hole to propagate down the plasma column and back. Increasing the amplitude of the hole causes a decrease in the hole propagation speed, as shown by the open circles in Fig. 7. The positive voltage step on R3 used to excite the hole causes a slight lengthening of the plasma column. The resulting fractional length increase is measured to be at most about 2%, which is not explicitly subtracted out of the calculation of the propagation speed.

As the excitation voltage on ring R3 increases to above 12 V, a density hole with a leading edge forms. This leading edge breaks off from the main hole, becomes a smaller hole, and propagates ahead of the main hole with a faster speed. The first and second traces shown in Fig. 8 demonstrate this process occurring. In some instances where the step pulse on R3 exceeds about 18 V (not shown in the figure), smaller

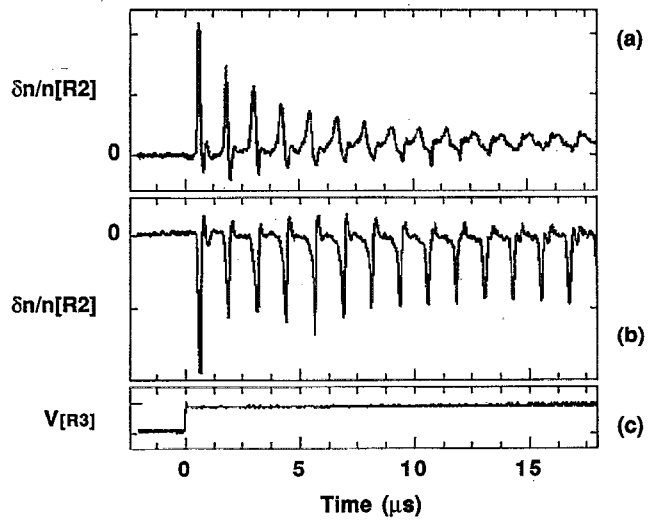

FIG. 9. Long time behavior of (a) an electron plasma soliton and (b) an electron hole measured on R1. The peak amplitude corresponds to a density perturbation of about 10%. (c) The measured voltage pulse on R3 that produces the electron hole.

holes are sloughed off both ahead and behind the main density hole. Measurement of the parallel electron distribution function of the plasma column following the excitation of a moderate amplitude electron hole indicates a slight increase in the distribution in an energy range roughly corresponding to the propagation speed of the hole. This indicates the presence of trapped electrons in the hole.

Figure 9 shows the long-time behavior of the electron soliton [Fig. 9(a)] and hole [Fig. 9(b)]. Both objects tend to last for many bounce periods in the plasma column. The soliton is substantially Landau damped in about ten periods; in contrast, the electron hole is very stable and is damped only after 50–100 periods. A physical explanation for this difference is based on the interaction between the electrons and the potential of the soliton or hole. The soliton presents a positive energy barrier to all passing electrons. Some electrons with velocities sufficiently near the soliton velocity such that they cannot overcome the positive energy barrier are reflected in the forward or backward direction by the soliton, causing either an increase or decrease in the energy and momentum of the soliton. There are more electrons reflected in the forward direction for a plasma in thermal equilibrium. This causes a decrease in the energy and momentum of the soliton so that the overall effect is a damping of the soliton. In contrast, the hole presents a negative energy barrier to all passing electrons. As a result, the damping of the hole is not a result of electron reflections but a result of kinetic effects that are not yet well understood experimentally or theoretically.

We studied interactions between holes and solitons by creating two separate soliton–hole pairs at either end of the plasma column and colliding them. Even though the soliton and hole from each initial pair evolve separately (i.e., the hole–soliton pair is not a single nonlinear object consisting of a hole and soliton that stay together for a long time), they preserve their identity even after many collisions with the

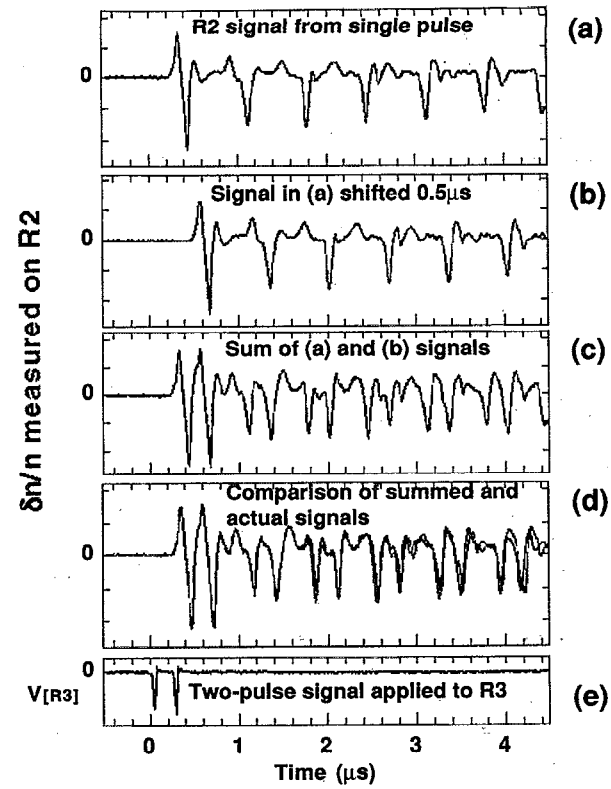

FIG. 10. Signal traces measured on ring R1 showing the result of repeated collisions between an electron hole and soliton with another electron hole or soliton. (a) Electron hole–soliton produced with only the first 50 ns pulse shown in (e). (b) Electron hole–soliton produced with only the second 50 ns pulse shown in (e); this is the same signal as in (a), but delayed 0.5 μs. (c) The algebraic sum of signals (a) and (b) showing the expected signal for collisions with no interaction. (d) The algebraic sum in (c) compared with the actual signal produced with the two pulses in (e) showing a slight difference occurring late in time. (e) Measured voltage applied to ring R3.

other hole and soliton. Measurements show that after about five or six collisions there appears a small displacement in the hole and soliton position from their position when no collisions take place. This result is similar to measurements of neutral plasma solitons, which also show a displacement in the soliton's position (along the direction of motion) after a collision with another soliton.

Propagation and collisions between electron solitons and holes are shown in Figure 10. First, a single negative pulse lasting for 50 ns is applied to R3 to produce the R2 signal shown in Fig. 10(a). Shortly after $t=0$ this trace shows a sharp positive density bump immediately followed by a sharp negative density bump (there is an additional small positive bump after this). This positive and negative bump combination represents a soliton–hole pair. The soliton is produced by the negative step in the excitation pulse, and the hole is produced by the positive step 50 ns later. The soliton–hole pair appear as a second positive and negative bump after one bounce off the plasma end and are smaller in amplitude than at the start. Following the trace further in time shows the positive bump arriving more and more early than the negative bump and both decreasing in amplitude. The hole and soliton behave independently as the soliton

(positive signal) is seen to move ahead of (separate from) the hole (negative signal) with increasing time.

Collisions between holes and solitons are observed when two negative pulses are applied to R1, as shown in Fig. 10(e). The delay of 500 ns between pulses is chosen so that the first pair has time to reach the opposite end of the column when the second pair is launched. Figure 10(b) is the signal of Fig. 10(a) shifted by 500 ns; this shows how the second soliton–hole pair would evolve alone. Figure 10(c) is the algebraic sum of the first two traces. This is the expected signal on R1 if the two soliton–hole pairs propagate completely independently of each other. The signal received on R2 from an actual two-pulse experiment is shown as Fig. 10(d), overlaid with the summed signal. The overlaid traces agree very closely except at long times, where the peaks and valleys of the interaction trace occur slightly earlier in time than the peaks and valleys of the summed trace. This means that collisions between the holes and solitons lead to a slight forward displacement for both holes and solitons. Previous measurements of ion acoustic soliton collisions show that two colliding solitons both receive small displacements in the forward direction during a collision. We have experimentally demonstrated that a similar result holds for two colliding holes, solitons, or a colliding hole and soliton in the pure electron plasma. The 500 ns time separation between excitation pulses is such that repeated collisions between density perturbations with oppositely directed velocities occur near the middle of the plasma column. Finally, this result demonstrates that a soliton or hole can collide with another soliton or hole and preserve its identity in the pure electron plasma. Note that here, all collisions are between oppositely traveling disturbances.

In spite of the many similarities between solitons and holes in neutral and pure electron plasmas, we have observed a number of differences. For example, the spatial width of the electron soliton seems to slightly increase for a greater soliton amplitude rather than decrease as is observed in neutral plasma solitons. In addition, the electron hole observed in this system does not exhibit a threshold for excitation as is observed in neutral plasmas; it can be excited with a potential that ranges continuously down to zero. Similarly, the hole speed is typically close to the fastest electron plasma wave phase speed (two to three times the electron thermal speed), whereas the neutral plasma holes have a speed close to the electron thermal speed. Also, the speed of electron holes decreases with hole amplitude, whereas in neutral plasmas, the hole speed tends to increase with increasing excitation potential.

The cause of these differences has not been experimentally investigated in detail here. One possible cause for some of these differences may be that the holes and solitons studied here are excited using a conducting ring with a short axial length (the axial length is only one-half of the ring diameter). This is in contrast to previous experiments on neutral plasmas, which make use of a grid or a long conducting cylinder for hole or soliton excitation. The excitation potential from a short ring is very different than the potential created by a grid or a long cylinder, and this may affect the hole or soliton dynamics.

Summarizing the electron hole and soliton observations we find that electron holes or solitons are produced by applying a positive or negative step voltage to ring R2. The resulting density perturbations are 16–20 cm long and propagate with a speed that depends on the perturbation amplitude. The soliton Landau damps in about 5–10 transits of the apparatus, whereas the electron hole propagates for 50–100 transits. At large amplitudes, the soliton is accompanied by a free-streaming electron burst. A large-amplitude hole tends to slough off a smaller hole, which then propagates ahead of the main hole. An electron soliton or hole preserves its identity in a collision with either another electron soliton or hole.

VI. CONCLUSIONS

We have experimentally investigated the rarefaction wave produced by the free expansion of a magnetized pure electron plasma column along the axial magnetic field. The rarefaction front propagates into the undisturbed plasma column at the phase speed of the long-wavelength electron plasma waves. The plasma flow behind the rarefaction front is self-similar in nature, so the plasma density and velocity profiles in this region have no characteristic length scale. This absence of length scale sets the free expansion apart from other large-amplitude plasma disturbances, which possess definite length scales such as a soliton, electron hole, or a shock wave. The density behind the rarefaction front approaches an intermediate plateau level, and remains near this level until the rarefaction front returns from reflection off of the confined end of the plasma column. The plasma density then decreases from the plateau value to zero as the remaining plasma empties from the confinement region.

A noninteracting neutral gas model, which keeps only the kinetic effects in the free expansion, does not predict the measurements well, although the prediction is improved for a warm plasma. The new hydrodynamic model, which retains pressure and electrostatic effects, shows good agreement with both cold and warm plasma measurements. The fluid model successfully predicts the measured density plateau level and the shape of the rarefaction front.

Electron solitons and holes in the pure electron plasma are similar to their counterparts in a neutral plasma. Both objects have density scale lengths of several plasma diameters; they exhibit an amplitude-dependent speed, and they persist for long times in the plasma, although the soliton damps more quickly than the electron hole. Collisions between an electron hole or soliton and another hole or soliton show that each object preserves its identity in the collision but experiences a small forward position shift. Several differences between neutral solitons and holes and pure electron solitons and holes were described

ACKNOWLEDGMENTS

One of the authors (J.D.M.) would like to acknowledge fruitful discussions with Dr. F. J. Moody whose expertise in fluid dynamics proved invaluable in understanding the re-

sults reported here. In addition, helpful discussions with Dr. T. M. O'Neil, Dr. D. Dubin, and Dr. R. A. Smith are gratefully acknowledged.

This work is supported by U.S. Department of Energy Grant No. DE-FG03-85ER53199.

[1]H. Ikezi, P. J. Barrett, R. B. White, and A. Y. Wong, Phys. Fluids **14**, 1997 (1971).
[2]V. I. Karpman, J. P. Lynov, P. Michelsen, H. L. Pécseli, J. Juul Rasmussen, and V. A. Turikov, Phys. Rev. Lett. **43**, 210 (1979); Phys. Fluids **23**, 1782 (1980).
[3]J. P. Lynov, P. Michelsen, H. L. Pécseli, J. Juul Rasmussen, K. Saeki, and V. A. Turikov, Phys. Scr. **20**, 328 (1979).
[4]K. Saeki, P. Michelsen, H. L. Pécseli, and J. Juul Rasmussen, Phys. Rev. Lett. **42**, 501 (1979).
[5]H. Schamel, Phys. Scr. **20**, 336 (1979).
[6]M. Kako, T. Taniuti, and T. Watanabe, J. Phys. Soc. Jpn. **31**, 1820 (1971).
[7]K. Saeki and H. Ikezi, Phys. Rev. Lett. **29**, 253 (1972); K. Saeki, J. Phys. Soc. Jpn. **35**, 251 (1973).
[8]Ch. Sack and H. Schamel, Phys. Fluids **29**, 1337 (1986) and references therein.
[9]J. E. Allen and L. M. Wickens, J. Phys. **40**, C7-547 (1979).
[10]A. V. Gurevich, L. V. Pariĭskaya, and L. P. Pitaevskiĭ, Sov. Phys. JETP **22**, 449 (1966).
[11]J. E. Crow, P. L. Auer, and J. E. Allen, J. Plasma Phys. **14**, 65 (1975).
[12]A. H. Shapiro, *The Dynamics and Thermodynamics of Compressible Fluid Flow* (Ronald, New York, 1953), pp. 128–131 and 462–528.
[13]*Non-Neutral Plasma Physics*, Proceedings of the Symposium of Non-Neutral Plasma Physics, Washington, DC, 1988, edited by C. W. Roberson and C. F. Driscoll, AIP Conf. Proc. No. 175 (American Institute of Physics, New York, 1988), pp. 1–74.
[14]Although the distance between the edges of rings G1 and S2 is 107.5 cm the plasma length is shorter than this as a result of the electrostatic confinement potential that extends beyond the edge of the ring and keeps the plasma end about 3 cm away.
[15]J. D. Moody and J. H. Malmberg, Bull. Am. Phys. Soc. **34**, 1933 (1989).
[16]J. H. Malmberg and C. B. Wharton, Phys. Rev. Lett. **17**, 175 (1966).
[17]A. W. Trivelpiece and R. W. Gould, J. Appl. Phys. **30**, 1784 (1959).
[18]M. Abramowitz and I. A. Stegun, *Handbook of Mathematical Functions* (Dover, New York, 1972), Chap. 7.
[19]D. M. Moody, J. Fluid Mech. **214**, 455 (1990).
[20]W. M. Manheimer, Phys. Fluids **12**, 2426 (1969).
[21]L. D. Landau and Lifshitz, *Fluid Mechanics*, 2nd ed. (Pergamon, New York, 1987), p. 366.
[22]The fastest electron plasma wave is the one with no radial nodes in the radial eigenfunction.
[23]F. J. Moody, *Introduction to Unsteady Thermofluid Mechanics* (Wiley, New York, 1990), pp. 253–285, and 444–454.
[24]J. D. Moody and J. H. Malmberg, Phys. Rev. Lett. **69**, 3639 (1992).